


***Ab initio* study of the structural response to magnetic disorder and van der Waals interactions in FeSe**Felix Lochner,^{1,2} Ilya M. Eremin², Tilmann Hickel¹, and Jörg Neugebauer¹¹Max-Planck-Institut für Eisenforschung, D-40237 Düsseldorf, Germany²Institut für Theoretische Physik III, Ruhr-Universität Bochum, D-44801 Bochum, Germany (Received 9 July 2020; revised 10 January 2021; accepted 1 February 2021; published 15 February 2021)

The electronic structure in unconventional superconductors holds a key to understanding the momentum-dependent pairing interactions and the resulting superconducting gap function. In superconducting Fe-based chalcogenides, there have been controversial results regarding the importance of the k_z dependence of the electronic dispersion, the gap structure, and the pairing mechanisms. Here, we use density functional theory to investigate the underlying structural properties in combination with a sophisticated real-space treatment of magnetic disorder for the prototype system FeSe. Our calculations demonstrate that interlayer and intralayer interactions need to be considered and that charge-driven van der Waals interactions between Se atoms instead of magnetic coupling effects drive the interlayer binding. The methodological advances and physical insights are important for upcoming investigations of the three-dimensional effects, including nontrivial topology, of FeSe_{1-x}Te_x and FeSe_{1-x}S_x systems.

DOI: [10.1103/PhysRevB.103.054506](https://doi.org/10.1103/PhysRevB.103.054506)**I. INTRODUCTION**

Among several types of Fe-based superconductors (FeSCs) discovered so far, FeSe has the simplest crystal structure consisting only of superconducting layers. This system turns out to be unique not only due to its structural properties but also due to the lack of any magnetic transition at ambient pressure [1]. The tetragonal-to-orthorhombic structural transition at $T_s \approx 90$ K [2,3], where the orthorhombic structure is called the nematic phase analog to liquid crystals [4], occurs in FeSe without the presence of any ordered magnetic state [2,5]. In addition, the interplay of physical pressure and chemical substitution causes dramatic changes in the phase diagram [6–9]. This underlines the delicate interplay between real-space crystal structure and the electronic properties including magnetism in this compound.

Although electronic correlations are relatively strong in Fe-based superconductors, the application of density functional theory (DFT) has proven to reliably provide insights into their physics. The band structure calculations correctly predict the main electronic properties for most of the Fe-based superconductors including their Fermi surface topology, their structural and magnetic transitions, and the possible strength of electron-phonon interactions [10]. The projection of DFT results onto Wannier functions, based on symmetry considerations, further yields low-energy models that can be used to analyze the broken symmetries in these systems [11,12].

In most of the Fe-based superconductors the magnetic ground state is in DFT and experiment given by the C -type antiferromagnetic order, often called the stripe-type antiferromagnetic (sAFM) order [13–15]. Previous DFT works on FeSe also predict the sAFM state as the ground state [16]. In experiment, however, this magnetic phase appears only at

finite pressure, while at ambient pressure the so-called nematic (structural) transition without any long-range magnetic order is observed [2,3,17,18]. The resulting complex pressure-dependent phase diagram is highly debated [19]. Several *ab initio* calculations explained the absence of the long-range magnetic order by the presence of competing magnetic phases with different ordering vectors [20]. The resulting magnetic frustration prevents the formation of the long-range magnetic order but allows the nematic transition, which is breaking Z_2 symmetry [21–24]. Moreover, a clear impact of the nematic transition on the magnetism in the material indicates a strong coupling between the structure and spin fluctuations [25,26].

Observe also that superconductivity in FeSe is quite sensitive to structural modifications, in particular, to the height of the Se atoms above the iron layer, z_{Se} [27] (see Fig. 1). Thus the three-dimensional aspects of superconductivity, which are often ignored, as well as the physics explaining the deviation of calculated lattice parameters from the experimental ones are of high interest. In particular, there are indications that dynamic dipole-dipole [van der Waals (vdW)] interactions might be important, as they drive interlayer attraction [27–29].

Although there are several *ab initio* publications on the magnetic phases, structural stabilities, and vdW interactions [21,28,29], the combined study of the interplay of magnetic interactions in the paramagnetic state and the vdW forces on the electronic structure and structural parameters in FeSe is so far missing. One of the requirements to correctly capture the low-temperature physics of the nematic state in DFT is to avoid long-range magnetic order and consider a paramagnetic (PM) state instead. Sometimes the nonmagnetic (NM) state is considered to represent a sufficient PM setup; however, ignoring the magnetic moments is physically not correct, and it gives even worse results of the real-space structure [29].

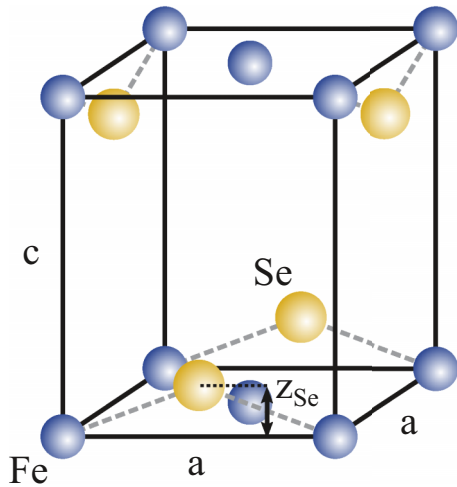


FIG. 1. Atomic structure of tetragonal FeSe. The three structural parameters that have to be relaxed are the a and c lattice constants as well as z_{Se} , i.e., the height of the Se atoms with respect to the iron layer.

Therefore, in this paper, we employ a real-space spin space averaging based on special quasirandom structures [30]. Besides the new insights into the interplay of magnetic and real-space phase stabilities achieved in this paper, this approach can serve as a benchmark for other DFT-based studies that use ordered magnetic states instead [1,21].

Based on the foundation of a correct magnetic description, we evaluate the vdW interactions in FeSe. A few *ab initio* investigations have already indicated structural improvements by including a vdW correction [28,29]. However, they have neither considered the sensitive interplay with magnetism, which is the focus of our study, nor analyzed the physical nature of the vdW contribution in FeSe. In this paper we present a side-by-side investigation of two dedicated vdW approaches [31,32], which allows us to systematically explore the impact of vdW interactions on structural parameters and to resolve the important interdependence of interlayer and intralayer corrections. In particular, we investigate an isolated layer of FeSe in a vacuum, which is the best way to separate the impact of intralayer interactions from that of the interlayer interactions. We believe that the in-depth understanding of the interplay between electronic, magnetic, and structural degrees of freedom obtained here for FeSe can also be used in a variety of other FeSCs.

The paper is organized as follows. In Sec. II we describe the PM and vdW extensions to standard DFT calculations. In Sec. III, first the implementations of both extensions are treated separately, and then the combination of the PM and vdW extensions is investigated. Moreover, a study of the electronic dispersion is presented. Finally, we summarize our results in Sec. IV.

II. METHODS

A. Paramagnetism

In contrast to experiment, standard DFT predicts the sAFM state to be stable in FeSe and is commonly used although

other magnetic states are close in energy [29]. Due to this degeneracy the competition of several magnetic configurations may yield frustration and prevent the stability of long-range magnetic order in FeSe [21]. It is well known that the presence of magnetic order and disorder has a strong effect on the structural properties of Fe-based materials [33]. This calls for a systematic study within the PM state to investigate the structural behavior of the system in the nematic phase without long-range magnetic order and with higher precision. In particular, we construct different special quasirandom structures (SQSs) to maximize the magnetic disorder in a finite simulation box. This approach is based on geometrical considerations and determines for a given real-space structure the best possible collinear spin configuration to mimic the PM state. For FeSe we distinguish three species (Se atoms, Fe-up atoms, and Fe-down atoms), where the SQS is performed for the Fe atoms. Hereby, we used the Alloy Theoretic Automated Toolkit (ATAT) package [30] to create three different setups of the magnetic moments. The difference of those SQSs is the real-space cutoff radii for the correlations considered in the construction algorithm. To make a systematic treatment of the magnetism possible, the magnetic moments of each Fe atom have the same magnitude.

Due to convergence issues with automatized relaxation algorithms for the ionic positions and the magnetic moments, the height of Se atoms with respect to the iron layer (z_{Se}), the volume, and the c -to- a ratio (c/a) are relaxed sequentially. Moreover, constrained magnetic moments are used, where both direction and magnitude are constrained, to avoid NM final structures.

To calculate the local magnetic moments, an integral over a sphere Ω_i , which depends on a radius given by the chosen structure and the volume of the unit cell (UC) in particular, is taken. This system-specific radius is chosen in such a way that 98% of the UC is used for evaluating the magnetic moment, which also leads to an overlap of some of those spheres within the UC.

To get the magnetic moment m_{opt} that is energetically preferred by the system, we fit the total energy to a polynomial function

$$f(m) = \alpha m^2 + \beta m^4 \quad \text{with } \alpha, \beta \in \mathbb{R}, \quad (1)$$

which is the simplest form of the Landau free-energy expansion.

B. Selected van der Waals implementations

FeSe is a compound with strongly different polarizabilities; thus the distribution of Fe and Se atoms yields different interlayer and intralayer vdW contributions. Therefore we have carefully investigated the interdependence of vdW interactions and modifications of all lattice parameters. In order to resolve this interdependence, we have chosen two different vdW approaches. On the one hand, we employ the DFT-D2 approach of Grimme [31], referring to dispersion correction version 2, which is a conceptually more simple approach. On the other hand, we employ the DFT-TS approach of Tkatchenko and Scheffler [32], which includes the desired geometrical weighting based on the compound used. These approaches represent different levels of complexity and will

make the differences between the interlayer and intralayer vdW interactions visible. For FeSe the DFT-D2 method has already been used; a detailed comparison with the DFT-TS method, however, is so far missing [28,29]. While for details about the individual approaches we refer to Refs. [31,32], we focus the upcoming discussion on the differences between the DFT-D2 method and the DFT-TS method.

In general, the vdW interactions are introduced by adding a semiphenomenological correction E_{vdW} to the standard DFT energy by

$$E_{\text{vdW}} = -\frac{s}{2} \sum_{A,B}^{N_{\text{at}}} f_{\text{dmp}}(R_{AB}) \frac{C_{6,AB}}{R_{AB}^6}, \quad (2)$$

where s is a global scaling factor depending on the chosen exchange-correlation functional (see Ref. [31] for details). N_{at} describes the total number of atoms in the unit cell, where R_{AB} refers to the distance between different atoms A and B . $C_{6,AB}$ is the corresponding C_6 parameter of the polarizability, and f_{dmp} is a global damping function.

The main difference between the two approaches is the choice of the $C_{6,AB}$ parameters. For DFT-D2, least-squares fits of experimentally found atomic C_6 parameters given by the dipole oscillation strength distribution method (DOSD) are used [34], and a geometric mean, $C_{6,AB} = \sqrt{C_{6,A}C_{6,B}}$, is taken for binary contributions [31]. This by construction ignores the specific atomic configuration in a given system. For example, in the case of FeSe the intralayer Se-Se interaction is calculated without including the underlying Fe layer.

For the DFT-TS method the $C_{6,AA}$ parameters are derived from the parameters for one freestanding atom (“at”) of the same species given by

$$C_{6,AA} = \frac{\eta_A}{\eta_A^{\text{at}}} \left(\frac{\kappa_A}{\kappa_A^{\text{at}}} \right)^2 \left(\frac{V_A}{V_A^{\text{at}}} \right)^2 C_{6,AA}^{\text{at}}. \quad (3)$$

Here, all quantities without the index “at” refer to effective parameters of the full system. The $C_{6,AA}^{\text{at}}$ are taken from Ref. [35], and η is an effective frequency (introduced in the London formula [36]). The effective volume $V_A = \kappa_A \alpha_A$ (κ_A is a scaling factor for the polarizability α_A) dresses the C_6 parameter by including the local environment in the form

$$\frac{\kappa_A \alpha_A}{\kappa_A^{\text{at}} \alpha_A^{\text{at}}} = \frac{V_A}{V_A^{\text{at}}} = \frac{\int r^3 w_A(\mathbf{r}) n(\mathbf{r}) d^3 \mathbf{r}}{\int r^3 n_A^{\text{at}}(\mathbf{r}) d^3 \mathbf{r}}, \quad (4)$$

with the Hirschfeld atomic partitioning weights [37]

$$w_A(\mathbf{r}) = \frac{n_A^{\text{at}}(\mathbf{r})}{\sum_B n_B^{\text{at}}(\mathbf{r})}. \quad (5)$$

The sum over $n_B^{\text{at}}(\mathbf{r})$ is the so-called promolecule electronic density. As a combination rule for C_6 parameters, DFT-TS uses the expression

$$C_{6,AB} = \frac{2C_{6,AA}C_{6,BB}}{\frac{\alpha_B}{\alpha_A} C_{6,AA} + \frac{\alpha_A}{\alpha_B} C_{6,BB}}. \quad (6)$$

C. Computational details

All calculations are performed using the Vienna *Ab Initio* Simulation Package (VASP) [38–40] with the projector augmented wave method [41] and exchange-correlation functionals of Perdew-Burke-Ernzerhof [42] type.

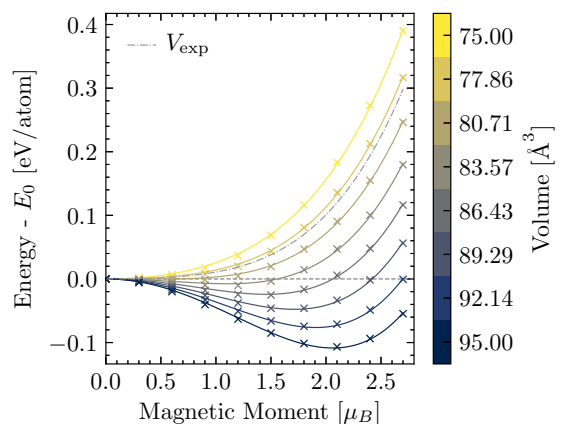


FIG. 2. Fe-atom magnetic-moment-dependent total energy of spin constrained DFT-TS calculations aligned to its energy of zero magnetization. The polynomial fits are obtained from Eq. (1). The color bar shows the chosen volumes. The gray dash-dotted curve indicates the dependency for the experimental volume at 298 K [46].

Calculations for the UC use a $12 \times 12 \times 8$ Monkhorst-Pack k -point mesh [43]. The energy cutoff is set to 450 eV, justified by a convergence of the bulk modulus to a precision of 1%. For the electronic smearing we chose first-order Methfessel-Paxton smearing [44] with $\sigma = 0.1$ eV. The PM calculations are performed in a $2 \times 2 \times 2$ supercell with a $6 \times 6 \times 4$ k -point mesh accordingly. We also compared a $2 \times 2 \times 2$ supercell with a $3 \times 3 \times 3$ supercell to investigate the influences of finite size effects. Here, only small changes in energy and for the magnetic moments of the Fe atoms are observable (as described in the next section).

For the calculations of the isolated layer (IL) setup in Sec. III C, the distance of the FeSe layers is 30 Å, while the vdW interaction length is set to 20 Å. This suppresses interlayer vdW interactions without influencing intralayer ones. The k points in the c direction are significantly increased to ensure a sufficient mapping of interlayer effects.

Setting up all calculations, postprocessing, and analyzing are done by using the integrated development environment PYIRON [45].

III. NUMERICAL RESULTS

A. Paramagnetic calculations

To investigate the disordered magnetic phase, we constrain the magnetic moments of the Fe atoms as described in the previous section. To compare the influence of disorder to the structural properties, we also calculate the structural parameters for the sAFM state for comparison. As explained later in this section, the cell shape in the PM calculations corresponds to a quasiequilibrium and is not fully converged. Since the differences in structure and energy for each calculation step are small, we took a snapshot after nine complete minimization steps for the following analysis.

The exemplary results for one employed SQS spin setup are illustrated in Fig. 2, where the fits are obtained by Eq. (1). Here, the transition from the NM state at $V = 75 \text{ \AA}^3$ to the PM state at $V = 95 \text{ \AA}^3$ can be clearly seen. Only by constraining the magnetic moments can the smooth phase transition

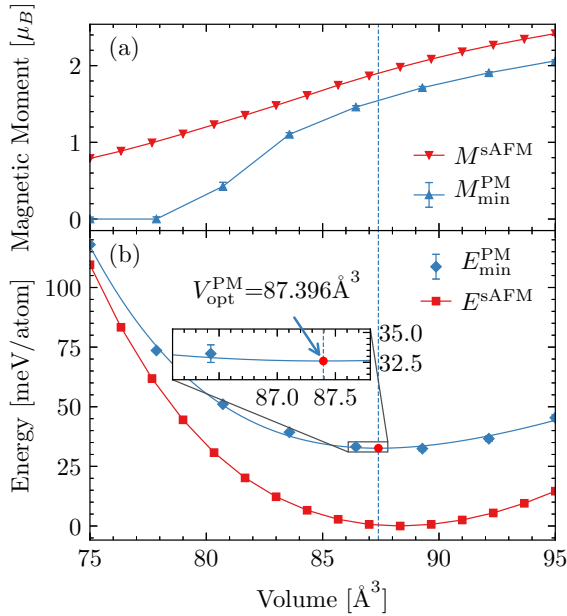


FIG. 3. (a) Magnetic moments and (b) total energies per Fe atom as obtained at the minima of the fits in Fig. 2 compared with the sAFM state (red solid curves) for the same structural parameters. The error bars are connected to the fit, the dashed line indicates the optimal volume for the SQS configuration as obtained by the Rose-Vinet equation of states [47], and the fit is shown by the solid curves.

be investigated. Extracting the minimal energy values and corresponding magnetic moments, we calculate the quasiequilibrium volume for each SQS.

Since several SQSs are required to get sufficient statistics for the PM average, the energy-volume curves for the mean of three SQSs are shown for one exemplary relaxation step in Fig. 3(b). Since there is almost no scatter between the different structures, the setup for the SQS (i.e., the size of the supercell) is sufficient to describe the PM ground state. In addition, the changes in structural parameters due to an increase in the size of the supercell to $3 \times 3 \times 3$ is comparable to these differences between SQS structures.

Moreover, the obtained fit to the Rose-Vinet equation of states [47] is in good agreement with the given data, confirming a smooth transition from the PM ($V \approx 87 \text{ \AA}^3$) to the NM ($V \approx 80 \text{ \AA}^3$) ground state. We learn from Fig. 3(a) that the quasiequilibrium state has a finite magnetic moment, while the NM state is unstable. The larger error bar for the intermediate volumes ($V \approx 81 \text{ \AA}^3$) between the PM and NM states reflects the competition of these phases, when both are close in energy. Those errors, however, do not show a large influence on the Rose-Vinet fit, which means that PM calculations are still sufficiently reliable even in the regions of comparably small magnetic moments. Also the mean magnetic moment of the Fe atoms at the quasiequilibrium lattice constant ($M_{\text{opt}}^{\text{PM}} \approx 1.6 \mu_B$) is comparable for PM and sAFM ($M_{\text{opt}}^{\text{sAFM}} \approx 1.8 \mu_B$). We see a small variation of the magnitude of the magnetic moments for the Fe atoms in the PM state. This might be related to several magnetic sublattices with different absolute magnetic moments, as discussed for the 11-compounds previously [48]. As the variation is in the

tolerance of the approach used, we consider this effect to be less important for the structural parameter relaxation.

It should also be noticed that the total energy per atom at the quasiequilibrium for the PM state is about 30 meV larger than that for the sAFM state. This indicates that the PM state is not the ground state in the present DFT approach but would become stabilized by magnetic entropy. However, the PM calculations include constrained magnetic moments; thus the total energy includes a penalty which is also in the order of 10 meV. Since a competition of several short-range magnetic orders is also considered to drive the PM state in the nematic region [20], it might also explain the remaining difference as ordered states are usually lower in energy.

It is important to note that by introducing the PM state, the already weak interlayer interactions in the sAFM state are further reduced such that no stable distance of the FeSe layers exists. The resulting quasifree behavior of the layers indicates that magnetic interactions are not able to explain the interlayer coupling in this compound for the disordered magnetic state. Therefore our results show that vdW forces are mandatory to stabilize bulk FeSe in the PM regime (see Sec. III C). This is in contrast to the sAFM state, where a stabilization is observed also without vdW interactions. Here, a magnetic coupling is expected, since the comparable magnitude of the magnetic moments of the Fe atoms in the PM and sAFM states makes an explanation of interlayer attraction by covalent bonds questionable. This difference in the magnetic effect raises further questions about the role of third dimensionality in superconductivity in FeSe; yet the existence of strong vdW forces in FeSe has been reported earlier [27–29].

B. van der Waals calculations

To account for the interlayer attraction mentioned in the previous section, we include vdW forces for the PM state. In order to quantify the physical impact of vdW corrections, however, we first need to apply them to a state that is already structurally stable, i.e., the sAFM state. Moreover, we calculate the structural response for the DFT-D2 approach as well as the DFT-TS approach, as they decouple the interlayer and intralayer interactions differently. We analyze the performance of these methods by studying the response to volume and shape changes for FeSe.

1. Total energies

In DFT and *ab initio* thermodynamics it is common to analyze the energetics of materials as a function of volume. For the volume-dependent calculations we relax the cell shape as well as the ionic positions simultaneously [49]. If electronic interlayer and intralayer interactions are of the same origin and magnitude, the ratio between the lattice constants a and c is expected to change only weakly after a cell-shape relaxation. Moreover, z_{Se} should be proportional to changes in the volume.

The total energy in Fig. 4 shows a shallow minimum for non-vdW sAFM. Since the binding is too small to explain a stability at moderate temperatures, the magnetic interlayer interactions apparently underestimate the overall interlayer attractions also for this state. In contrast, both DFT-D2 and DFT-TS show a clear minimum at $V_{\text{min}}^{\text{D2}} =$

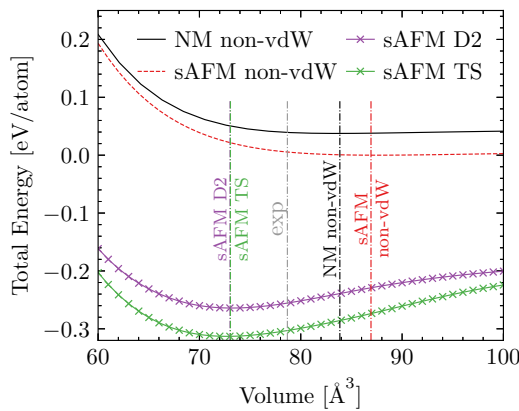


FIG. 4. Calculated total energy vs volume for the non-vdW NM state (black solid curve) and non-vdW sAFM state (red dashed curve) compared with vdW corrected sAFM calculations by the DFT-D2 (D2) method (violet solid curve) and the DFT-TS (TS) method (green solid curve). The values are aligned to the minimum of the total energy of the non-vdW sAFM curve. The dash-dotted lines indicate the experimental (exp) volume at 298 K in Ref. [46] (gray), the non-vdW optimized volume for NM (black) and sAFM (red), and the optimized volume for the sAFM DFT-D2 approach (violet) and the sAFM DFT-TS approach (green).

73.022 Å³ and $V_{\min}^{\text{TS}} = 73.059$ Å³. The corresponding volumes are smaller than the non-vdW optimized volume at $V_{\min}^{\text{non-vdW}} = 86.931$ Å³, which is about ≈ 10 Å³ larger than the experimentally measured volume [46] [see Fig. 6(a)]. We will discuss below to what degree the nearly similar optimal volumes for DFT-D2 and DFT-TS are a coincidence or indicating the similarity of the implemented physical concepts. For non-vdW calculations the deviation of the lattice constant a from the experimental value is only about 1%, and yet the lattice parameter c is $\sim 13\%$ too large. This indicates that the failure of the uncorrected DFT Hamiltonian primarily affects the interlayer interactions. As discussed below the smaller vdW corrected volume can be explained by an overestimation of intralayer interactions.

The insufficient interlayer interaction for non-vdW calculations is also reflected in the bulk modulus $B_0^{\text{non-vdW}} = 3.86$ GPa, which is approximately an order of magnitude smaller than the vdW values of $B_0^{\text{DFT-D2}} = 30.12$ GPa and $B_0^{\text{DFT-TS}} = 33.12$ GPa. The latter are in the same region as the experimental values [50,51]. A minor effect is the volume expansion due to temperature. Since the experimental values are measured at room temperature, the volume at $T = 0$ K will be reduced. Indeed, other works on 11-compounds show that the volume decreases with decreasing temperature [52].

2. Structural distortion

Next we systematically analyze the structural impact of the volume reduction from the non-vdW optimized volume at $V_{\min}^{\text{non-vdW}} = 86.931$ Å³ to the corrected volume. As can be seen in Fig. 5 the difference between DFT-D2 and DFT-TS is more pronounced along this path than the equilibrated values observed in Fig. 4.

In the first place, the reduction in volume is connected with a reduction in c/a , as can be seen in Fig. 5(c). We note in this context that in the non-vdW curve the lattice parameters a and z_{Se} are nearly constant above $V^{\text{non-vdW}}$, while the lattice parameter in the c direction steadily increases. Thus the Fe layers drift apart, due to the vanishing interlayer bonds as also observed for the PM calculations in Sec. III A and known as the exfoliation of graphene [53]. The substantial overestimation of c/a in the non-vdW approach is, therefore, due to the missing interlayer interactions in this volume region.

Having understood this, it is remarkable that the DFT-D2 approach has a qualitatively different impact on c/a than the DFT-TS approach. In the former case, c/a is, in comparison with the non-vdW calculations, even enhanced next to $V^{\text{non-vdW}}$. This is caused by the reduction in the lattice parameter in the a direction in Fig. 5(b) and a resulting increase in the lattice parameter in the c direction in Fig. 5(a). The overestimate of the intralayer interaction is a direct consequence of the vdW correction within the DFT-D2 approach but is less pronounced in the DFT-TS approach for this volume region. Here, the c value decreases as expected by a vdW correction,

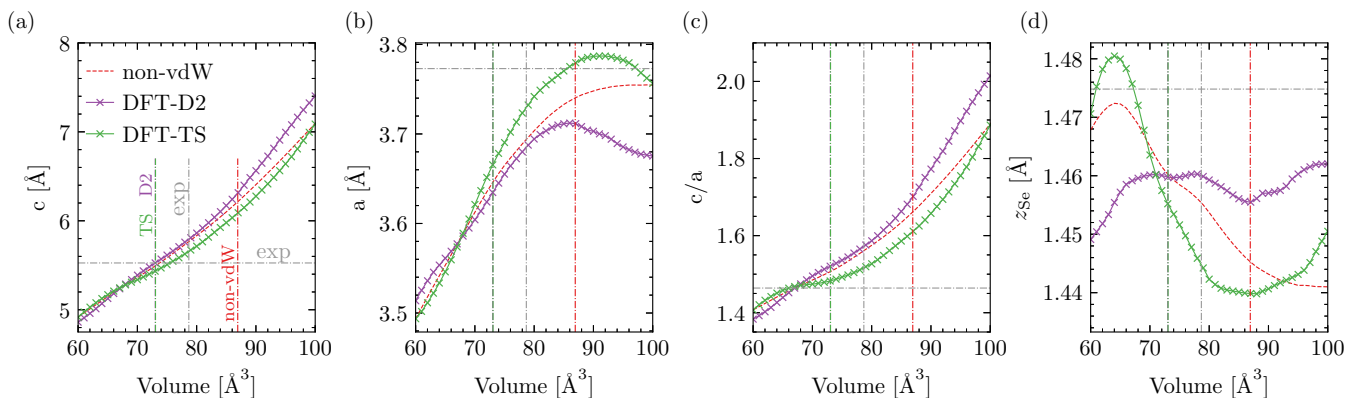


FIG. 5. Volume dependence of the sAFM state for standard DFT calculations (red dashed curves) compared with vdW corrected ones by the DFT-D2 (violet solid curves) and DFT-TS (green solid curves) methods of (a) the lattice parameter in the c direction, (b) the lattice parameter in the a direction, (c) the fraction of lattice parameters c and a , and (d) the height of Se atoms above the iron plane (z_{Se}). The dash-dotted lines indicate the experimental values in Ref. [46] (gray), the non-vdW optimized volume (red), and the optimized volumes for the DFT-D2 approach (violet) and the DFT-TS approach (green).

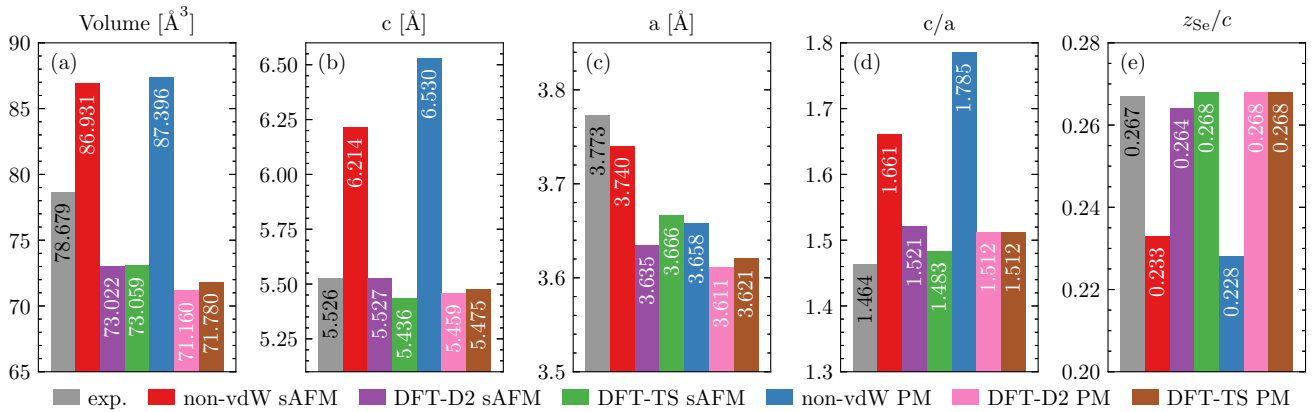


FIG. 6. Lattice parameters for FeSe in the sAFM and PM states with and without vdW corrections. The experimental values in Ref. [46] (gray) and the numerical values for non-vdW sAFM calculations (red), sAFM DFT-D2 calculations (violet), sAFM DFT-TS calculations (green), non-vdW PM calculations (blue), PM DFT-D2 calculations (pink), and PM DFT-TS calculations (brown) are illustrated for (a) the minimum volume of the UC, (b) the lattice parameter in the c direction, (c) the lattice parameter in the a direction, (d) the fraction of lattice parameters c and a , and (e) the height of the Se atom z_{Se} in units of c .

and the increase in the lattice parameter a might be caused by a Poisson effect. The z_{Se} parameter in Fig. 5(d) shows a roughly antiproportional trend compared with the lattice parameter a ; thus the bond length tries to remain constant. A similar effect will also be discussed in the context of Figs. 6 and 7 below.

When approaching the experimental volume at $V_{\text{min}}^{\text{exp}} = 78.679 \text{ \AA}^3$, the slopes of the c/a for the vdW approaches are reduced compared with the region of higher volumes. This effect is now strongest for the DFT-TS method. As the cell is compressed, the overestimated intralayer vdW attraction causes a stronger decrease in the lattice parameter a , whereas the value in the c direction is less influenced. Here, z_{Se} for

the DFT-TS method varies significantly, while its value in the DFT-D2 approach shows only moderate changes.

In the volume region around $V \approx 70 \text{ \AA}^3$, which is close to the vdW optimized volumes of DFT-D2 and DFT-TS, the structural parameters (i.e., the c/a) for both methods are similar. Therefore the effects of interlayer and intralayer vdW corrections are comparable for both approaches. The difference in the total energy, however, is still large (see Fig. 4).

By looking at the complete volume region, the DFT-D2 and DFT-TS approaches, i.e., their different treatment of the geometrical composition, imply significantly different behaviors.

The investigation of both vdW implementations shows that the vdW interactions can be well separated into interlayer and intralayer ones. Thus the quality of the structural relaxations in the a direction and the c direction has to be treated independently. Due to the additional contribution of the Hirschfeld partitioning in the DFT-TS approach, in particular, the intralayer interaction becomes relevant in a different volume region than for the DFT-D2 approach. The z_{Se} parameter is within DFT-D2 for large volumes close to the experimental value, but the largely reduced gradient of z_{Se} with respect to volume compared with DFT-TS indicates a cancellation of interactions. Similar to the assessment of exchange-correlation functionals in DFT [54], the good agreement of the vdW approaches close to their equilibrium volumes increases confidence in the vdW corrections. One should, however, keep in mind that the intralayer interactions are overestimated in both approaches at the equilibrium volume.

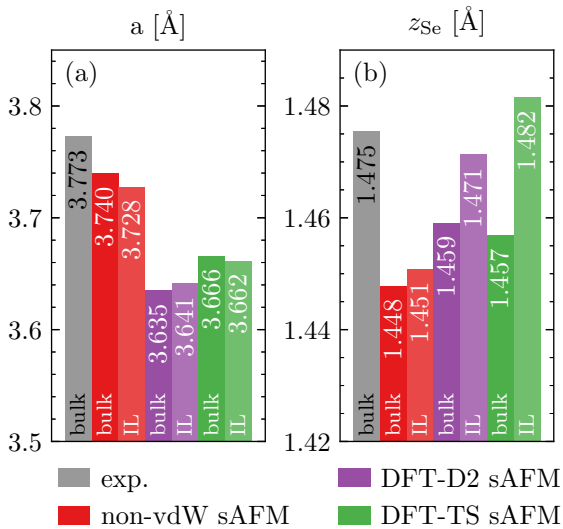


FIG. 7. Lattice parameters for bulk FeSe and an isolated layer (IL) of FeSe in the sAFM state with and without vdW corrections. The experimental values in Ref. [46] (gray) and the numerical values for non-vdW sAFM calculations (red), sAFM DFT-D2 calculations (violet), and sAFM DFT-TS calculations (green) are illustrated for (a) the lattice parameter in the a direction and (b) the height of the Se atom z_{Se} .

C. Combined studies of paramagnetic and van der Waals calculations

As outlined above, the combination of PM calculations with van der Waals corrections is the most accurate DFT treatment of FeSe. As an extension of Sec. III B, we will now discuss the impact of this combination on the different structural parameters. Due to the numerical effort of PM calculations, this discussion is limited to the optimized volume. To analyze the actual influence of magnetic and charge-based

interactions, a benchmarking against approaches without this combination is performed.

1. Structural parameters

The structural parameters in Fig. 6 demonstrate an overall very good agreement of the combined approach with the experimental values for both the DFT-D2 and the DFT-TS corrections. In contrast to the non-vdW PM calculations, the minimization of the total energy in the PM state results in a well-defined equilibrium volume, due to the correct description of the interlayer binding. In particular, the $z_{\text{Se-to-}c}$ ratio (z_{Se}/c) is in nearly perfect agreement with the experimental value for both vdW implementations [see Fig. 6(e)]. The origin of this is a reduction in the lattice parameter in the c direction and the c/a [see Figs. 6(b) and 6(d)] as a direct consequence of the improved interlayer attraction.

As shown above, the vdW corrections work as effectively for the PM state as they work for the sAFM state. This indicates the strength of the vdW interactions compared with the magnetic ones. Thus it is also most likely that the driving forces of interlayer interaction are not dominated by magnetism, but by charge-based Se-Se interactions. This becomes particularly clear when inspecting the c lattice parameter and the c/a in Figs. 6(b) and 6(d). Comparing first the non-vdW corrected lattice parameter for the PM and the sAFM states, it can be seen that the lattice parameter in the c direction is significantly increased. The optimized volume is nearly constant, since a reduction in the lattice constant in the a direction completes the distortion. The underlying reason is the reduced magnetic interlayer coupling in the PM state, which results in a structural instability. As soon as the vdW corrections are taken into account, however, the c lattice constant is in both cases reduced to almost the same parameter. This indicates that the stronger magnetic coupling in the sAFM state is not required for the structural stability.

Similarly, by looking at Fig. 6(e), it can be seen that z_{Se}/c for the PM state does not show any significant changes compared with the sAFM state. This underlines again that the interlayer attraction is solely caused by the presence of vdW interactions and can only be correctly reproduced by DFT calculations if they are taken into account. It also shows that the magnetic ordering does not influence the structural parameters. As a consequence, it does no harm for the important z_{Se} coordinate if the magnetically much simpler structure of the sAFM state instead of the correct PM state is used in the calculations.

A consequence is, however, that also the lattice parameters of the vdW corrected PM calculations in the a direction are $\approx 3\%$ smaller than the experimental ones. As we have revealed in Sec. III B, this is mainly a result of the overestimated intralayer interactions. This shortcoming for the sAFM case remains similar in the PM calculations. In order to provide a possible solution, we now revisit the discussion of interlayer vs intralayer interactions in the context of optimized volumes.

2. Isolated layer

To investigate the intralayer interactions in detail, we additionally calculate an isolated FeSe layer in a vacuum, i.e., a case where by construction no interlayer interactions occur.

These calculations are performed for the sAFM state only, due to the limited impact of magnetic ordering on the intralayer structural parameters.

In Fig. 7(a) it can be seen that the relaxed lattice parameter a for the bulk compound and the IL do not show a significant difference. Thus the overbinding in the a direction is mostly caused by the intralayer vdW interactions. This result clearly shows that both approaches work well to include vdW bonding when other bond types such as covalent or ionic are absent. However, these approaches do not consider the reduction in vdW interactions when other bond types are present, as is the case for intralayer interactions.

While the intralayer lattice constant a is almost identical for the bulk and the IL, the two systems show a pronounced difference in the internal structure parameter z_{Se} . Switching the interlayer interactions off increases this parameter systematically compared with the bulk compound [see Fig. 7(b)]. Thus the interlayer interactions off increases this parameter systematically compared in the c direction of the FeSe layers. Since these interactions are mostly driven by the vdW attraction of the Se atoms, we consider the ratio z_{Se}/c rather than the bare z_{Se} displacement to analyze structural improvement in Fig. 6(e). However, the analysis of the non-vdW effect on the bare z_{Se} displacement yields a dominant magnetic effect. This also becomes apparent when comparing with NM calculations, for which the z_{Se} coordinate is only 1.387 (with vdW) or 1.383 Å (without vdW).

The investigation of the IL shows that the lattice parameters in the a direction (mainly driven by intralayer non-vdW interactions) and the c direction (mainly driven by interlayer vdW interactions) are decoupled. Thus the non-vdW calculations provide a sufficiently accurate description of lattice parameter a , whereas vdW corrected calculations are mandatory to describe the lattice parameter c . To simultaneously improve both quantities, a vdW implementation would be needed that takes the effect of strong covalent bonds on the vdW interaction into account. A possible approach to remove overbinding by vdW corrections is to perform the sum in Eq. (2) only over the pairs of atoms that are in different layers. Since this requires a new implementation of vdW in the DFT code, we did not test it.

D. Band dispersion

To investigate the electronic band dispersion, we use the optimized structural parameter of the sAFM state for our investigations, since the parameters for sAFM and PM are quite similar and of better reproducibility. We take NM calculations with structural parameters obtained by experiments [46] (see Fig. 6) as a reference. Although the NM state and the sAFM state differ for the structural parameters, their band dispersions are very similar except for some slight differences [see Fig. 8(a)]. For example, the k_z dependence of the Se p_z orbital, which crosses the Fermi surface (FS) along $\Gamma \rightarrow Z$, is stronger for the experimental values, and the Fe $3d$ orbitals are mostly k_z independent. As a result we find a similar shape of electron pockets around the M point and the A point of the Brillouin zone and flatter dispersions from the Γ point to the Z point, which is due to d_{xz} and d_{yz} orbitals along the $\Gamma \rightarrow Z$ direction.

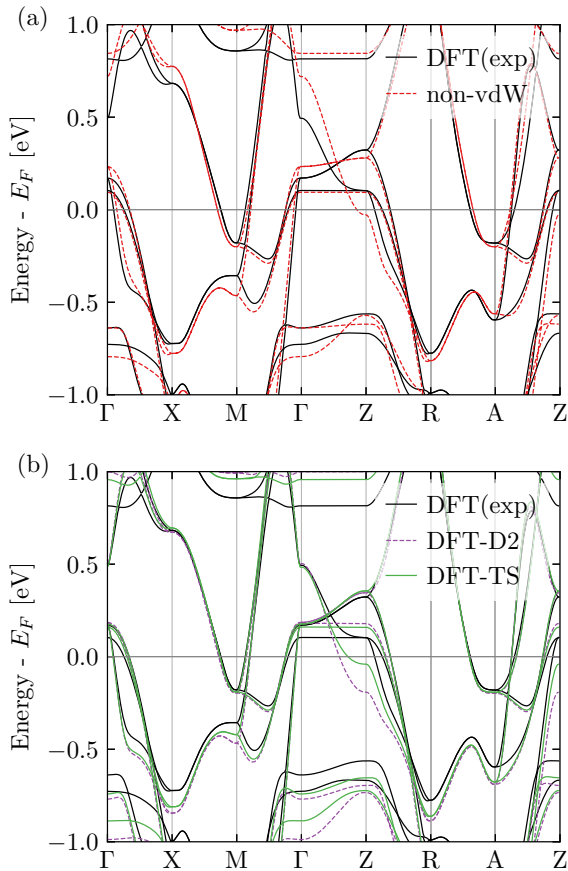


FIG. 8. Electronic band dispersion near the Fermi energy obtained by nonmagnetic DFT calculations for the different lattice parameters given in Fig. 6. Specifically, non-vdW DFT calculations using experimental lattice parameters in Ref. [46] (black solid curves) and (a) the non-vdW sAFM state (red dashed curves) as well as (b) DFT-D2 vdW (violet dashed curves) and DFT-TS vdW (green solid curves) corrections are given.

For the vdW corrected calculations the changes in the real-space structure are also reflected in the electronic dispersion. Comparing the band dispersion with and without vdW corrections, a sizable k_z dependence of the Fe $3d$ orbitals is indeed found, consistent with previous works [28]. Additionally, the shape of the electron pockets for $k_z = \pi$ is the same as for calculations with the experimental lattice parameters, a clear improvement to non-vdW sAFM calculations. Although other works propose interlayer-driven effects on the band dispersion to be less important for superconductivity, a reconstruction of the FS by the Se p_z -orbital-dominated band from $\Gamma \rightarrow Z$ is found [27]. This may be related to an overestimation of interlayer Se attraction.

Comparing both vdW approaches for FeSe (presumptive for all 11-based FeSCs), the electronic band dispersions turn out to be very similar. Most important is the enhancement of

the interlayer interaction, which is in agreement with considerations of other works claiming vdW interactions to be important for FS reconstructions [27]. The DFT-TS approach includes the impact of the local environment on the vdW interaction, slightly reducing the overestimation of the intralayer interaction in DFT-D2 and improving the z_{Se}/c . The only noticeable consequence in the band dispersion, however, is a modified band energy near the FS at the Z point.

IV. SUMMARY

Based on a systematic DFT study, we show that the delicate interplay between magnetic and vdW interactions is crucial for the real-space structure and its stability in FeSe. By introducing a real-space PM setup based on the SQS method, we find structural instabilities in the ground state due to a lack of interlayer interactions. While the sAFM state stabilizes the lattice structure artificially, the physically correct way of ensuring interlayer coupling is the vdW interaction.

We further demonstrate that once vdW interactions are taken into account, the impact of magnetic order on the structural properties is small, because the charge-driven Se-Se interactions play a more important role than the magnetic Fe-Fe ones. The z_{Se} coordinate, which is important for superconducting properties, can only be correctly reproduced by DFT calculations that include vdW corrections and ensure that local magnetic moments are present but that do not give rise to a global magnetization. We therewith justify the approximate vdW calculations used in a few previous works [28,29].

The detailed investigation of the two most common vdW approaches, DFT-D2 and DFT-TS, and the study of an isolated layer in vacuum show that an interplay of interlayer and intralayer interactions determines the vdW corrections. While the interlayer binding is correctly considered with both vdW approaches, the intralayer vdW interaction seems to be overestimated. We therefore suggest a refined computational scheme that handles the two interactions separately.

By including vdW interactions, the introduced interlayer attraction makes FeSe a much more three-dimensional material, which is shown by our investigation of the electronic dispersion. This agrees with recent angle-resolved photoemission spectroscopy (ARPES) experiments [55]. The change of the character of the electronic dispersion from quasi-two-dimensional towards a more three-dimensional one with a significant contribution of the Se p_z orbitals is also relevant in the context of topological features, discussed previously [56], and needs to be explored further both experimentally and theoretically.

ACKNOWLEDGMENTS

We thank C. Freysoldt for fruitful discussions. We gratefully acknowledge financial support by the German Research Foundation within the DFG-ANR project MAGIKID (Grant No. HI1300/13-1) (F.L. and T.H.) and DFG Grant No. ER 463/14-1 (I.M.E.).

- [1] A. E. Böhmer and A. Kreisel, *J. Phys. Condens. Matter* **30**, 023001 (2018).
- [2] T. M. McQueen, A. J. Williams, P. W. Stephens, J. Tao, Y. Zhu, V. Ksenofontov, F. Casper, C. Felser, and R. J. Cava, *Phys. Rev. Lett.* **103**, 057002 (2009).
- [3] S. Margadonna, Y. Takabayashi, M. T. McDonald, K. Kasperkiewicz, Y. Mizuguchi, Y. Takano, A. N. Fitch, E. Suard, and K. Prassides, *Chem. Commun. (Cambridge, U. K.)* **2008**, 5607 (2008).
- [4] R. M. Fernandes and J. Schmalian, *Supercond. Sci. Technol.* **25**, 084005 (2012).
- [5] M. Bendele, A. Amato, K. Conder, M. Elender, H. Keller, H.-H. Klauss, H. Luetkens, E. Pomjakushina, A. Raselli, and R. Khasanov, *Phys. Rev. Lett.* **104**, 087003 (2010).
- [6] S. Medvedev, T. M. McQueen, I. A. Troyan, T. Palasyuk, M. I. Erements, R. J. Cava, S. Naghavi, F. Casper, V. Ksenofontov, G. Wortmann, and C. Felser, *Nat. Mater.* **8**, 630 (2009).
- [7] M. Bendele, A. Ichsanow, Y. Pashkevich, L. Keller, T. Strässle, A. Gusev, E. Pomjakushina, K. Conder, R. Khasanov, and H. Keller, *Phys. Rev. B* **85**, 064517 (2012).
- [8] J. P. Sun, K. Matsuura, G. Z. Ye, Y. Mizukami, M. Shimozawa, K. Matsubayashi, M. Yamashita, T. Watashige, S. Kasahara, Y. Matsuda, J.-Q. Yan, B. C. Sales, Y. Uwatoko, J.-G. Cheng, and T. Shibauchi, *Nat. Commun.* **7**, 12146 (2016).
- [9] K. Kothapalli, A. E. Böhmer, W. T. Jayasekara, B. G. Ueland, P. Das, A. Sapkota, V. Taufour, Y. Xiao, E. Alp, S. L. Bud'ko, P. C. Canfield, A. Kreyssig, and A. I. Goldman, *Nat. Commun.* **7**, 12728 (2016).
- [10] D. Guterding, S. Backes, M. Tomić, H. O. Jeschke, and R. Valentí, *Phys. Status Solidi B* **254**, 1600164 (2017).
- [11] H. Eschrig and K. Koepf, *Phys. Rev. B* **80**, 104503 (2009).
- [12] F. Lochner, F. Ahn, T. Hickel, and I. Eremin, *Phys. Rev. B* **96**, 094521 (2017).
- [13] D. C. Johnston, *Adv. Phys.* **59**, 803 (2010).
- [14] H. Hosono, A. Yamamoto, H. Hiramatsu, and Y. Ma, *Mater. Today (Oxford)* **21**, 278 (2018).
- [15] P. Dai, *Rev. Mod. Phys.* **87**, 855 (2015).
- [16] Y.-F. Li, L.-F. Zhu, S.-D. Guo, Y.-C. Xu, and B.-G. Liu, *J. Phys. Condens. Matter* **21**, 115701 (2009).
- [17] R. Khasanov, K. Conder, E. Pomjakushina, A. Amato, C. Baines, Z. Bukowski, J. Karpinski, S. Katrych, H.-H. Klauss, H. Luetkens, A. Shengelaya, and N. D. Zhigadlo, *Phys. Rev. B* **78**, 220510(R) (2008).
- [18] F.-C. Hsu, J.-Y. Luo, K.-W. Yeh, T.-K. Chen, T.-W. Huang, P. M. Wu, Y.-C. Lee, Y.-L. Huang, Y.-Y. Chu, D.-C. Yan, and M.-K. Wu, *Proc. Nat. Acad. Sci. USA* **105**, 14262 (2008).
- [19] A. E. Böhmer, K. Kothapalli, W. T. Jayasekara, J. M. Wilde, B. Li, A. Sapkota, B. G. Ueland, P. Das, Y. Xiao, W. Bi, J. Zhao, E. E. Alp, S. L. Bud'ko, P. C. Canfield, A. I. Goldman, and A. Kreyssig, *Phys. Rev. B* **100**, 064515 (2019).
- [20] K. Liu, Z.-Y. Lu, and T. Xiang, *Phys. Rev. B* **93**, 205154 (2016).
- [21] J. K. Glasbrenner, I. I. Mazin, H. O. Jeschke, P. J. Hirschfeld, R. M. Fernandes, and R. Valentí, *Nat. Phys.* **11**, 953 (2015).
- [22] M. H. Christensen, J. Kang, and R. M. Fernandes, *Phys. Rev. B* **100**, 014512 (2019).
- [23] H. Ruiz, Y. Wang, B. Moritz, A. Baum, R. Hackl, and T. P. Devereaux, *Phys. Rev. B* **99**, 125130 (2019).
- [24] B. Busemeyer, M. Dagrada, S. Sorella, M. Casula, and L. K. Wagner, *Phys. Rev. B* **94**, 035108 (2016).
- [25] Q. Wang, Y. Shen, B. Pan, X. Zhang, K. Ikeuchi, K. Iida, A. D. Christianson, H. C. Walker, D. T. Adroja, M. Abdel-Hafiez, X. Chen, D. A. Chareev, A. N. Vasiliev, and J. Zhao, *Nat. Commun.* **7**, 12182 (2016).
- [26] Q. Wang, Y. Shen, B. Pan, Y. Hao, M. Ma, F. Zhou, P. Steffens, K. Schmalzl, T. R. Forrest, M. Abdel-Hafiez, X. Chen, D. A. Chareev, A. N. Vasiliev, P. Bourges, Y. Sidis, H. Cao, and J. Zhao, *Nat. Mater.* **15**, 159 (2016).
- [27] D. Guterding, H. O. Jeschke, and R. Valentí, *Phys. Rev. B* **96**, 125107 (2017).
- [28] F. Ricci and G. Profeta, *Phys. Rev. B* **87**, 184105 (2013).
- [29] Q.-Q. Ye, K. Liu, and Z.-Y. Lu, *Phys. Rev. B* **88**, 205130 (2013).
- [30] A. Walle and G. Ceder, *J. Phase Equilib.* **23**, 348 (2002).
- [31] S. Grimme, *J. Comput. Chem.* **27**, 1787 (2006).
- [32] A. Tkatchenko and M. Scheffler, *Phys. Rev. Lett.* **102**, 073005 (2009).
- [33] I. Bleskov, T. Hickel, J. Neugebauer, and A. Ruban, *Phys. Rev. B* **93**, 214115 (2016).
- [34] Q. Wu and W. Yang, *J. Chem. Phys.* **116**, 515 (2002).
- [35] X. Chu and A. Dalgarno, *J. Chem. Phys.* **121**, 4083 (2004).
- [36] K. T. Tang, *Phys. Rev.* **177**, 108 (1969).
- [37] F. L. Hirschfeld, *Theor. Chim. Acta* **44**, 129 (1977).
- [38] G. Kresse and J. Hafner, *Phys. Rev. B* **47**, 558 (1993).
- [39] G. Kresse and J. Furthmüller, *Phys. Rev. B* **54**, 11169 (1996).
- [40] G. Kresse and J. Furthmüller, *Comput. Mater. Sci.* **6**, 15 (1996).
- [41] P. E. Blöchl, *Phys. Rev. B* **50**, 17953 (1994).
- [42] J. P. Perdew, K. Burke, and M. Ernzerhof, *Phys. Rev. Lett.* **77**, 3865 (1996).
- [43] H. J. Monkhorst and J. D. Pack, *Phys. Rev. B* **13**, 5188 (1976).
- [44] M. Methfessel and A. T. Paxton, *Phys. Rev. B* **40**, 3616 (1989).
- [45] J. Janssen, S. Surendralal, Y. Lysogorskiy, M. Todorova, T. Hickel, R. Drautz, and J. Neugebauer, *Comput. Mater. Sci.* **163**, 24 (2019).
- [46] T. M. McQueen *et al.*, *Phys. Rev. B* **79**, 014522 (2009).
- [47] P. Vinet, J. R. Smith, J. Ferrante, and J. H. Rose, *Phys. Rev. B* **35**, 1945 (1987).
- [48] M. N. Gastiasoro and B. M. Andersen, *Phys. Rev. B* **92**, 140506(R) (2015).
- [49] Although the full relaxation may lead in special cases to slightly different positions and energy values due to changing numbers of plane waves in the calculation, we do not find any significant changes of the structure compared with relaxing one quantity after another.
- [50] J. N. Millican, D. Phelan, E. L. Thomas, J. B. Leão, and E. Carpenter, *Solid State Commun.* **149**, 707 (2009).
- [51] S. Margadonna, Y. Takabayashi, Y. Ohishi, Y. Mizuguchi, Y. Takano, T. Kagayama, T. Nakagawa, M. Takata, and K. Prassides, *Phys. Rev. B* **80**, 064506 (2009).
- [52] C. Koz, S. Rößler, A. A. Tsirlin, S. Wirth, and U. Schwarz, *Phys. Rev. B* **88**, 094509 (2013).
- [53] M. J. Allen, V. C. Tung, and R. B. Kaner, *Chem. Rev. (Washington, DC)* **110**, 132 (2010).
- [54] B. Grabowski, T. Hickel, and J. Neugebauer, *Phys. Rev. B* **76**, 024309 (2007).
- [55] M. D. Watson *et al.*, *Phys. Rev. B* **91**, 155106 (2015).
- [56] P. Zhang, Z. Wang, X. Wu *et al.*, *Nat. Phys.* **15**, 41 (2019).